methods

Protein-sphingolipid interactions within cellular membranes[S]

Per Haberkant,* Oliver Schmitt,* F.-Xabier Contreras,* Christoph Thiele,[†] Kentaro Hanada,[§]
Hein Sprong,** Constanze Reinhard,[††] Felix T. Wieland,[1,]* and Britta Brügger[1,]*

Heidelberg University Biochemistry Center,* 69120 Heidelberg, Germany; Max Planck Institute of Molecular Cell Biology and Genetics,[†] 01307 Dresden, Germany; Department of Biochemistry and Cell Biology,[§] National Institute of Infectious Diseases, Tokyo 162-8640, Japan; Department of Membrane Enzymology,** Bijvoet Center and Institute of Biomembranes, Utrecht University, 3584 CH Utrecht, The Netherlands; and Center for Human Genetics,[††] Katholic University Leuven, 3000 Leuven, Belgium

Abstract Each intracellular organelle critically depends on maintaining its specific lipid composition that in turn contributes to the biophysical properties of the membrane. With our knowledge increasing about the organization of membranes with defined microdomains of different lipid compositions, questions arise regarding the molecular mechanisms that underlie the targeting to/segregation from microdomains of a given protein. In addition to specific lipid-transmembrane segment interactions as a basis for partitioning, the presence in a given microdomain may alter the conformation of proteins and, thus, the activity and availability for regulatory modifications. However, for most proteins, the specific lipid environment of transmembrane segments as well as its relevance to protein function and overall membrane organization are largely unknown. To help fill this gap, we have synthesized a novel photoactive sphingolipid precursor that, together with a precursor for phosphoglycerolipids and with photo-cholesterol, was investigated in vivo with regard to specific protein transmembrane span-lipid interactions. As a proof of principle, we show specific labeling of the ceramide transporter with the sphingolipid probe and describe specific in vivo interactions of lipids with caveolin-1, phosphatidylinositol transfer protein β, and the mature form of nicastrin. This novel photolabile sphingolipid probe allows the detection of protein-sphingolipid interactions within the membrane bilayer of living cells.—Haberkant, P., O. Schmitt, F-X. Contreras, C. Thiele, K. Hanada, H. Sprong, C. Reinhard, F. T. Wieland, and B. Brügger. **Protein-sphingolipid interactions within cellular membranes.** *J. Lipid Res.* 2008. **49:** 251–262.

Supplementary key words   sphingosine • photoactivatable • ceramide transporter • phosphatidylinositol transfer protein • caveolin • nicastrin

Alterations of protein-lipid microenvironments are suggested to contribute to an increasing number of pathological conditions, such as Alzheimer's, diabetes, and cardiovascular diseases. Specific protein-lipid interactions may control the steady-state localization and functional state of a given transmembrane protein. In addition, the lipid environment specific for a given endomembrane may influence the maturation (e.g., posttranslational modification) of a protein. On the other hand, the lipid composition of a given endomembrane may be controlled by the transport of individual molecular lipid species based on specific recognition by a membrane protein. Whereas the specificity and functions of protein-protein interactions constitute the overwhelming part of our present knowledge in molecular cell biology, less is known about the specificity of interactions within the bilayer of proteins with lipids.

Although a growing number of studies using photo-activatable lipids demonstrate specific protein-lipid interactions in biological membranes (recently reviewed in Ref. 1), the technical limitations of lipid reagents have hampered a more complete analysis of these interactions. A variety of photolabile lipid molecular species (such as radiolabeled photolabile gangliosides) were used to probe interactions of a given lipid with a protein in the membrane bilayer (reviewed in Ref. 2). Furthermore, by aminoacylation of the sphingosine backbone, defined photolabile molecular species of sphingolipids became available (3, 4). As a more general approach to probe membrane lipid classes, photolabile fatty acid derivatives were fed to cells and shown to be incorporated preferentially into phosphoglycerolipids (5).

Abbreviations: 10-ASA, 10-azi-stearic acid; Cer, ceramide; CERT, ceramide transporter; DRM, detergent-resistant membrane; FCS, fetal calf serum; MβCD, methyl-β-cyclodextrin; photoChol, photo-cholesterol; photoPC, photo-phosphatidylcholine; photoSph, photo-sphingosine; PI-TP, phosphatidylinositol transfer protein; PVDF, polyvinylidene difluoride; SM, sphingomyelin; UV, ultraviolet.

[1] To whom correspondence should be addressed.
  e-mail: felix.wieland@bzh.uni-heidelberg.de (F.T.W.);
  britta.bruegger@bzh.uni-heidelberg.de (B.B.)
[S] The online version of this article (available at http://www.jlr.org) contains Supplementary data in the form of 5 figures.

In a similar way, we aimed at a precursor for sphingolipids that covers the range of endogenous sphingolipids, including the variety of their molecular species.

Here, we report the synthesis of a novel radioactively labeled photoactivatable sphingosine derivative, [³H]D-*erythro*-photo-sphingosine (photoSph), which allows the specific study of protein-sphingolipid interactions in vivo. This sphingolipid precursor contains a photoactivatable diazirine group, producing a highly reactive carbene upon ultraviolet (UV) irradiation. Both radioactivity and the photoactive group reside in the sphingoid backbone. Thus, metabolism of this lipid precursor generates radioactive photolabile sphingolipids with a complete range of molecular species and allows the analysis of protein-lipid interactions within the lipid bilayer. Besides the incorporation of sphingosine into complex sphingolipids, sphingosine can be subjected to phosphorylation at the C1 hydroxyl group. This reaction is mediated by sphingosine kinase and generates sphingosine-1-phosphate as a second messenger, which affects many important intracellular processes, such as angiogenesis, cell proliferation, and apoptosis (for a recent review, see Ref. 6). Inactivation of sphingosine-1-phosphate signaling is initiated by the enzyme sphingosine-1-phosphate lyase, leading to irreversible degradation of this lipid. Effective incorporation of exogenous sphingosine into complex sphingolipids is thus critically dependent on intracellular sphingosine kinase and sphingosine-1-phosphate lyase activity. In addition, intracellular accumulation of exogenously added sphingosine could result in increased levels of sphingosine-1-phosphate. Likewise, increased levels of ceramide (Cer) could trigger apoptotic events (for a recent review, see Refs. 7, 8).

In contrast to most hitherto used sphingolipid probes, our photoactivatable sphingolipids are synthesized at the same cellular location as their natural counterparts and thus will follow their intracellular routes. In addition, with this precursor, only protein-sphingolipid interactions are detected, as the complete degradation of [³H]D-*erythro*-photoSph does not generate products that are both radioactive and photolabile.

We analyzed the metabolism of [³H]D-*erythro*-photoSph in various cell lines. The precursor is converted in vivo into photolabile analogs of the cellular sphingolipids, as demonstrated by radiolabeling experiments and mass spectrometric analysis. UV irradiation of cells fed with [³H]D-*erythro*-photoSph results in a pattern of labeled proteins distinct from that obtained with [³H]photo-cholesterol ([³H]photo-Chol) and [³H]photo-phosphatidylcholine ([³H]photoPC). Like endogenous sphingolipids, the photolabile analogs can be recovered from detergent-resistant membranes (DRMs) of labeled cells.

As a proof of principle, we demonstrate that addition to cells of [³H]D-*erythro*-photoSph results in UV-dependent labeling of the ceramide transporter (CERT). Exploring novel specific protein-sphingolipid interactions in vivo, we find a direct interaction of sphingolipids with caveolin-1 and phosphatidylinositol transfer protein (PI-TP) β. Strikingly, only the mature form of nicastrin, a

subunit of the γ-secretase core complex, is labeled by [³H]D-*erythro*-photoSph.

EXPERIMENTAL PROCEDURES

Unless stated otherwise, all chemicals were from the Sigma-Aldrich group (Taufkirchen, Germany). The following lipids were used as standards in TLC analyses: Cer (porcine brain), phosphatidylcholine (bovine liver), cerebrosides (porcine brain), sphingomyelin (SM; egg), and D-*erythro*-sphingosine (bovine brain) were from Avanti Polar Lipids. Glucosylceramide (bovine buttermilk) and a monosialoganglioside mix (bovine) were purchased from Matreya (Pleasant Gap, PA).

Antibodies

The following antibodies were used: SC-89, a rabbit polyclonal antibody raised against a peptide mapping at the N terminus of caveolin-1 of human origin (Santa Cruz Biotechnology, Inc.), a mouse monoclonal IgG2a anti-V5 antibody (R960-25; Invitrogen, Karlsruhe, Germany), a monoclonal anti-FLAG M2 antibody from Sigma (F1804), a rabbit polyclonal antibody against the luminal domain of p23 (Henriette) (9), a rabbit polyclonal antibody against flotillin (10), and a mouse monoclonal antibody against nicastrin (MAB5556; Chemicon).

Chemical synthesis of [³H]*erythro*-photoSph

See supplementary data.

Preparation of the [³H]photoChol-methyl-β-cyclodextrin-complex

The synthesis of [³H]photoChol and the preparation of the [³H]photoChol-methyl-β-cyclodextrin (MβCD) complex were performed as described (5).

Cell culture and transfection

CHO cells were grown in αMEM and COS7 cells in DMEM, each supplemented with 10% fetal calf serum (FCS). If indicated, cells were transfected using lipofectin as a transfection reagent according to the instructions of the manufacturer (Invitrogen). A total of 20 μg of cDNA and 100 μl of lipofectin were used to transiently transfect a subconfluent 10 cm dish of cultured cells.

Lipid analysis

To study the metabolism of [³H]D-*erythro*-photoSph, CHO cells were grown in 3 cm dishes. Cells were fed 0.1 μM (4 μCi in 2 ml of medium) [³H]D-*erythro*-photoSph in αMEM supplemented with 10% delipidized FCS. [³H]D-*erythro*-photoSph was added as ethanolic solution, with a maximum final concentration of ethanol in the medium of 0.5%. After labeling, cells were transferred to ice, washed with PBS, and harvested in 1 ml of PBS by scraping. Cells were pelleted by centrifugation (16,000 g, 5 min, 4°C) and resuspended in 10 μl of water. A total of 100 μl of methanol was added and the mixture was vortexed for 15 s Precipitated proteins were removed by centrifugation (16,000 g, 15 min, 4°C), and the supernatant was recovered. Radioactivity was determined by liquid scintillation counting. For TLC analysis, equal amounts of activity were applied to silica plates, and lipids were separated using chloroform-methanol-water (65:25:4, v/v/v) as the solvent system. Radioactive photolabile sphingolipids were visualized by digital autoradiography (β-Imager 2000; Biospace, Paris, France). Radioactivity associated with individual lipids was determined with β-Vision software (Biospace). To this end, the total
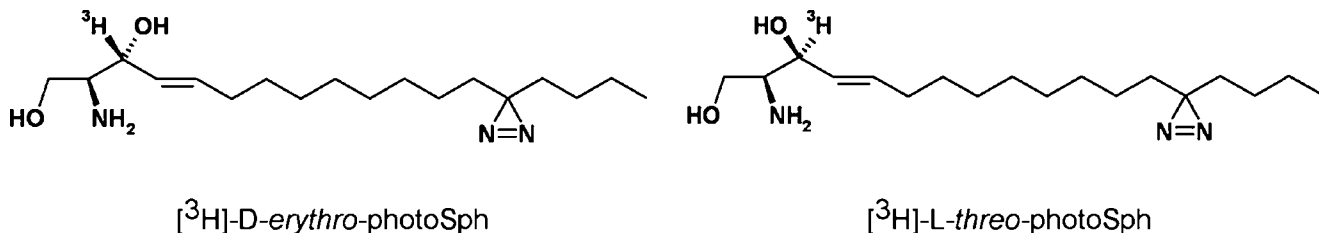
Fig. 1. Structures of [³H]D-*erythro*-photo-sphingosine (photoSph) and [³H]L-*threo*-photoSph. For details, see text.

number of events per lane and the number of events per individual spots were determined. See the supplementary data for mass spectrometric analysis of photoactivatable SM.

Photoaffinity labeling of cultured cells in vivo

Cells were grown in 10 cm dishes. If indicated, cells were transfected using lipofectin as a transfection reagent. For photoaffinity labeling studies, cells were washed with PBS, then medium containing lipid precursors was added. Media containing lipid precursors were prepared right before use: 0.2 mCi of MβCD-complexed [³H]photoChol was mixed with 10 ml of αMEM or DMEM containing 10% delipidized FCS; 0.2 mCi of an ethanolic solution of [³H]photoSph was lyophilized the day before use. The residue was dissolved in 50 μl of ethanol and mixed with 10 ml of αMEM or DMEM containing 10% delipidized FCS; 10-azi-stearic acid (10-ASA) was synthesized as described (5). A total if 0.2 mCi of an ethanolic solution of [methyl-³H]choline chloride (TRK 593; Amersham) was lyophilized and dissolved in 45 μl of ethanol and mixed with 5 μl of 100 mM 10-ASA in

ethanol. This solution was added to 10 ml of a choline-deficient αMEM or DMEM supplemented with 10% delipidized FCS. After labeling with the lipid precursor, the medium was removed and the cells were transferred to ice. All of the subsequent steps were performed at 4°C. Cells were washed with 10 ml of PBS, overlaid with 5 ml of PBS, and UV-irradiated (Sylvania R 100 W; UV-Labortechnik, Glashütten, Germany) for 15 min on ice. PBS was removed, and the cells were harvested in 1 ml of PBS by scraping. Cells were pelleted (16,000 *g*, 5 min) and lysed in lysis buffer [50 mM HEPES-NaOH, pH 7.4, 100 mM NaCl, 5 mM EDTA, 1% Triton X-100 (v/v), 0.5% deoxycholate (w/v), and protease inhibitor cocktail] for 1 h. After lysis, nuclei were removed by centrifugation (3,000 *g*, 10 min) and the supernatant was subjected to immunoprecipitation. Immune complexes were collected using protein A- or protein G-Sepharose beads, to which antibodies were covalently linked. A total of 180 μl of the cell lysate was subjected to immunoprecipitation. Beads were washed with lysis buffer (five times, 1 ml) and proteins were eluted using SDS-PAGE sample buffer. Samples were subjected to SDS-PAGE (10–20% gradient gel; Invitrogen) and Western blotting. Radio-
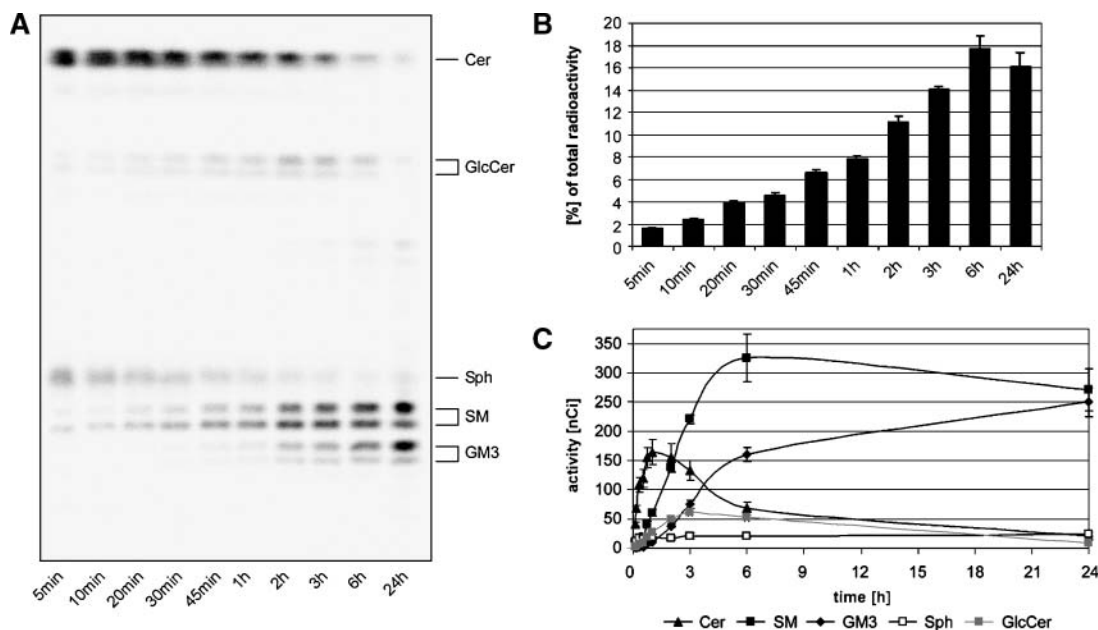

Fig. 2. Metabolism of [³H]D-*erythro*-photoSph in CHO cells. A 3 cm dish of CHO cells was labeled for different time periods with 0.1 μM (4 μCi/2 ml) [³H]D-*erythro*-photoSph. After labeling, cells were washed with cold PBS and scraped off. Cells were extracted with methanol as described. Radioactivity of lipid extracts was determined by liquid scintillation counting. A: Lipid extracts were analyzed by TLC using chloroform-methanol-water (65:25:4, v/v/v) as the solvent system; 0.025 μCi was applied per lane. Lipids were detected by digital autoradiography. Time of acquisition was 12 h. Lipid standards were used to identify individual spots. B: Recovery of radioactivity in lipid extracts, normalized to total radioactivity subjected to cells. C: Quantitation of radioactivity was performed using β-Imager software. Data are means ± SD of three different experiments. For details, see Experimental Procedures. Cer, ceramide; GlcCer, glucosylceramide; SM, sphingomyelin.

actively labeled proteins were visualized by digital autoradiography (β-Imager 2000; Biospace).

Preparation of DRMs

Two confluent 10 cm dishes of CHO cells ($\sim 1 \times 10^7$ cells) were labeled with 200 μCi (1 μM) of [^{3}H]D-erythro-photoSph in delipidized αMEM for 3 h. Cells were washed and mechanically harvested, and DRMs were prepared as described (11). Radioactivity in each fraction was determined by liquid scintillation counting. A total of 200 μl of each fraction was transferred to Wheaton tubes, and 400 μl of water was added. A total of 1.2 ml of chloroform-methanol (1:1, v/v) was added, and lipids were extracted. The organic layer was recovered. Equal volumes were applied to TLC. Lipids were separated using chloroform-methanol-water (65:25:4, v/v/v) as the solvent system. TLC plates were analyzed by digital autoradiography.

Analysis of lipids interacting with nicastrin

Fifteen centimeter dishes of SH-SY5Y cells were labeled for 6 h ([^{3}H]D-erythro-photoSph) or 18 h ([^{3}H]photoChol and [^{3}H]choline chloride/10-ASA) with 400 μCi of [^{3}H]D-erythro-photoSph, [^{3}H]photoChol, or [^{3}H]choline chloride/10-ASA in a total

volume of 20 ml as described above. Cells were transferred to ice, washed with 10 ml of PBS, and subjected to 10 min of UV irradiation. After UV irradiation, cells were scraped off and lysed in lysis buffer as described. Lysates were subjected to a dissociative immunoprecipitation using an anti-nicastrin antibody as described above. Five percent of input and 40% of the immunoprecipitated samples were separated by SDS-PAGE using a 10–20% Tris/Tricine gradient gel (Invitrogen). After transfer of proteins to polyvinylidene difluoride (PVDF) membranes, radioactively labeled proteins were visualized by digital autoradiography as described. Immunodetection was performed using an antibody directed against nicastrin.

RESULTS

Synthesis of photoactivatable [^{3}H]sphingosine

We describe the synthesis of a new photoactivatable sphingosine derivative containing a photolabile diazirine ring, [^{3}H]D-erythro-photoSph (**Fig. 1**). The total reaction scheme is depicted in supplementary Fig. I. Sodium borohydride reduction of protected 3-keto-14-azi-sphingosine
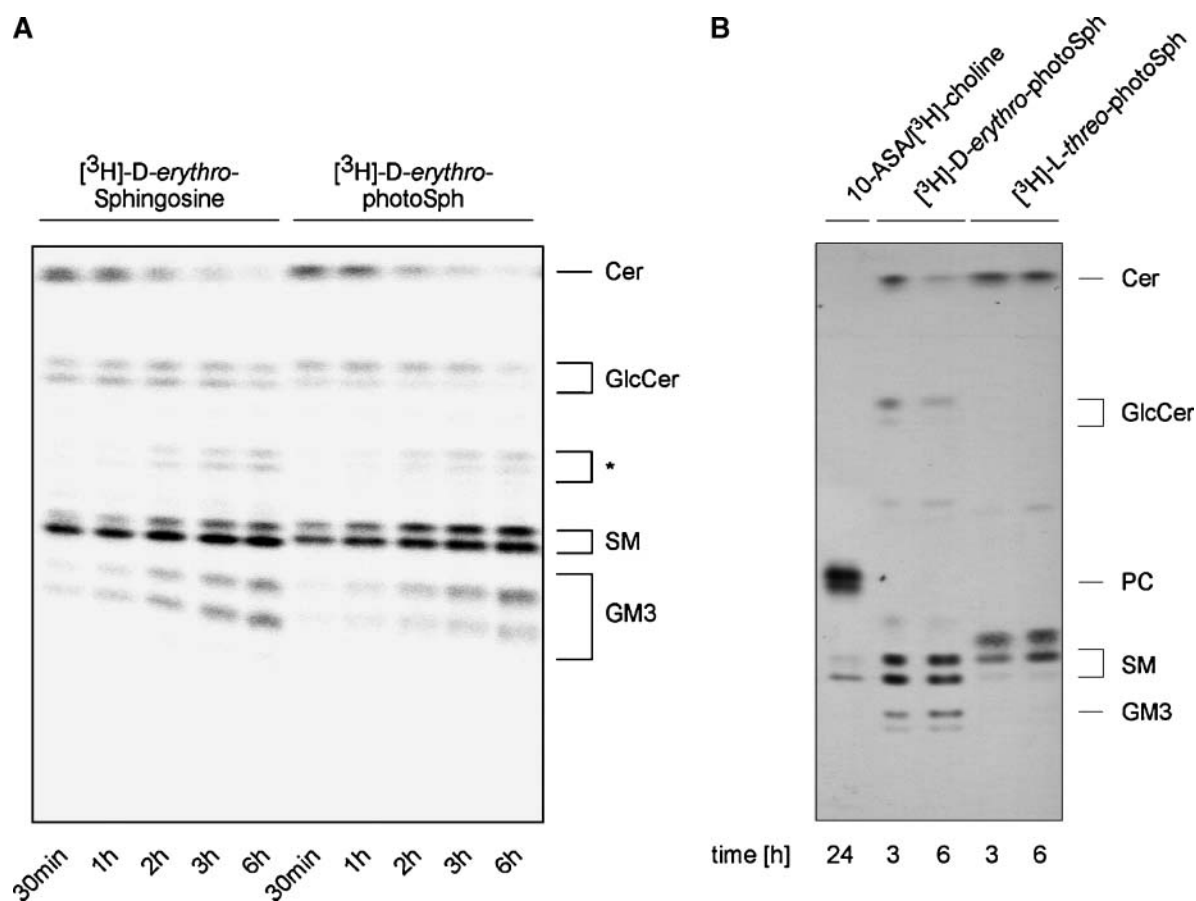

Fig. 3. Comparison of sphingolipid labeling using different lipid precursors. A: A 3 cm dish of CHO cells was labeled with 0.1 μM [^{3}H]D-erythro-photoSph or [^{3}H]D-erythro-sphingosine (4 μCi/2 ml). Lipids were extracted as described and analyzed by TLC (solvent system: chloroform-methanol-water, 65:25:4, v/v/v) and digital autoradiography (β-Imager). The asterisk indicates that lipid comigrates with phosphoethanolamine Cer standard. B: A 10 cm dish of CHO cells was labeled with 1 μM (200 μCi/10 ml) of either D-erythro- or L-threo-photoSph or with 50 μM 10-azi-stearic acid (10-ASA) per 100 μCi/10 ml choline chloride for different times. Lipids were resolved by TLC using chloroform-methanol-water (65:25:4, v/v/v) as the solvent system. The TLC plate was sprayed with Amplify Fluorographic Reagent (NAMP-100; Amersham) and exposed to Hyperfilm™ (HP79NA; Amersham Biosciences) at −80°C. A quantity of 0.05 μCi was applied per lane. For details, see Experimental Procedures.

generates two diastereomers: D-*erythro* (2*S*,3*R*)- and L-*threo* (2*S*,3*S*)-photoSph, with D-*erythro*-photoSph displaying the same stereochemistry as natural sphingosine. For the synthesis of radioactively labeled [³H]photoSph, [³H]sodium borohydride was used, generating [³H]L-*threo*-photoSph and [³H]D-*erythro*-photoSph (ratio, 0.3–0.5) with a specific activity of 20 Ci/mmol.

Cellular metabolism of [³H]D-*erythro*-photoSph

To analyze whether exogenously supplied photoSph is incorporated into sphingolipids, CHO cells were labeled with [³H]D-*erythro*-photoSph. To this end, cells were incubated with 0.1 μM (4 μCi) of this sphingolipid precursor for up to 24 h. Lipids were extracted and separated by TLC, and lipid patterns were analyzed by digital autoradiography. **Figure 2** shows the radioactive sphingolipid pattern obtained after distinct labeling times (see also supplementary Fig. II for analysis of COS-7 cells). The sphingosine-derived radioactivity was first recovered in Cer, which was then primarily converted into SM and glycosphingolipids. After 3 h of labeling, appreciable amounts of the various sphingolipid classes were detected. Prolonged labeling times shifted the incorporation of

the sphingosine-derived radioactivity into complex glycosphingolipids, showing that the introduction of the photolabile group does not interfere with the metabolic processing of the lipid precursor. Importantly, depending on the time of incorporation, labeling conditions can be chosen that shift the production of photoactivatable lipids to either photolabile Cer or photolabile glycolipids and SM (Fig. 2, compare 5 min and 24 h). In addition, the complexity can be resolved by applying appropriate labeling conditions along with specific sphingolipid inhibitors, thereby shifting the labeling toward one lipid class such as Cer or SM (see supplementary Fig. III).

We next compared the metabolic fate of [³H]D-*erythro*-photoSph and its radioactively labeled natural counterpart. CHO cells were labeled as indicated with [³H]D-*erythro*-photoSph or [³H]D-*erythro*-sphingosine for different time periods. Lipid extracts obtained from these cells were analyzed by TLC and digital autoradiography. As illustrated in **Fig. 3A**, the labeling patterns were comparable. We then compared the metabolism of [³H]D-*erythro*-photoSph and its nonnatural diastereomer [³H]L-*threo*-photoSph. Like [³H]D-*erythro*-photoSph, [³H]L-*threo*-photoSph was metabolized to photoCer and photoSM. As reported previously
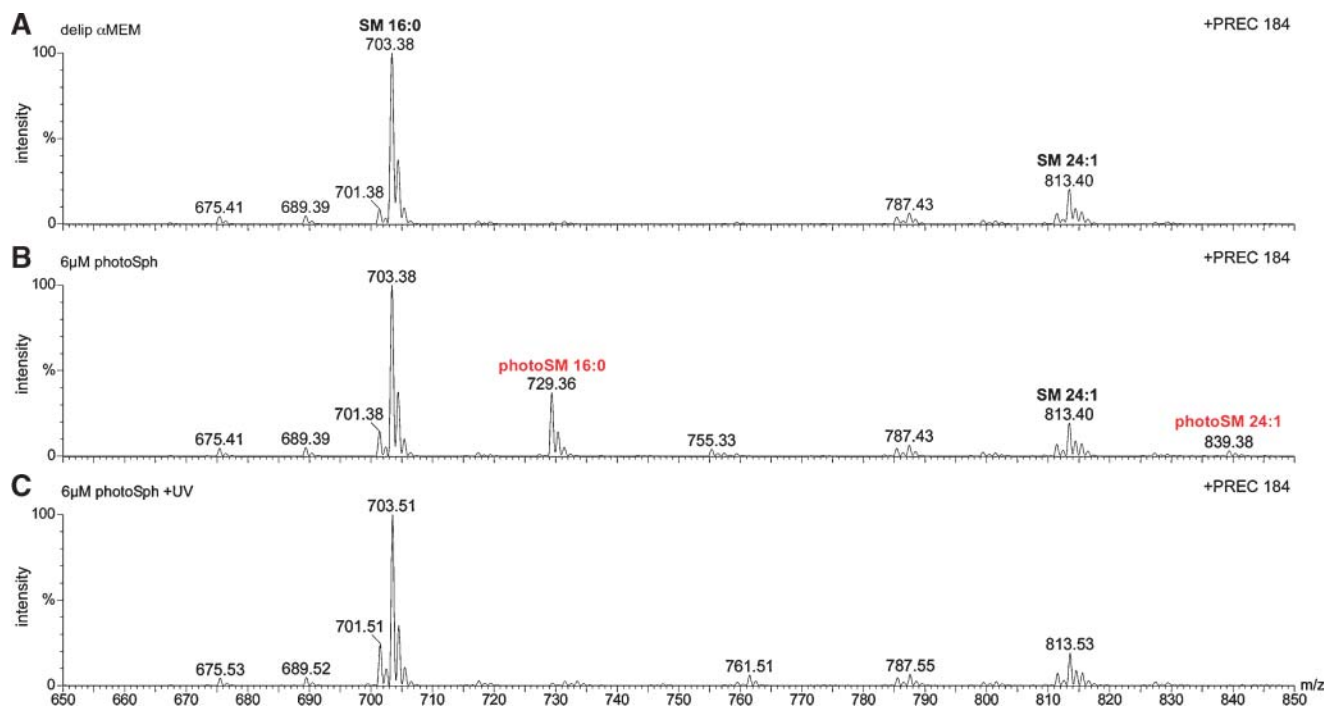

Fig. 4. Mass spectrometric analysis of photoactivatable SM. CHO cells (two 10 cm dishes, 1×10^7) were incubated for 3 h in delipidated medium in the absence (A) or presence (B) of 6 μM D-*erythro*-photoSph. Lipids were extracted, subjected to mild basic treatment to hydrolyze acyl-linked fatty acids of glycerophospholipids, and separated by TLC (solvent system: chloroform-methanol-water, 65:25:4, v/v/v) as described in Experimental Procedures. Lipid standards were used to identify individual sphingolipids. To analyze photoactive sphingolipids by mass spectrometry, silica of individual spots was recovered, followed by lipid extraction. Lipid extracts were dried and subsequently dissolved in 5 mM ammonium acetate in methanol and subjected to nano-ESI-MS/MS. A–C show PREC184 spectra of choline phosphate-containing lipids, selecting for precursor ions of *m/z* 184 Da and thus allowing the detection of positively charged choline phosphate-containing lipid species. Molecular masses are in Da, and the corresponding abbreviations give the total number of carbon atoms in the fatty acid attached to the sphingoid backbone and the numbers of double bonds within the fatty acid. A: PREC184 spectrum of a lipid extract obtained from CHO cells kept for 3 h in delipidated αMEM. B: Spectrum of a lipid extract from CHO cells labeled with 6 μM D-*erythro*-photoSph for 3 h. C: Spectrum of a lipid extract from B after the sample was irradiated with ultraviolet (UV) light.

(12), D-erythro-SM runs more slowly than L-threo-SM in the given TLC system. The conversion of [³H]L-threo-photoSph to SM was slower compared with [³H]D-erythro-photoSph. In contrast, [³H]L-threo-photoSph was not further metabolized to glucosylceramide or higher glycosphingolipids, as already described for L-threo-sphinganine, L-threo-sphingosine, and L-threo-Cer (13–15). Analysis of lipid extracts from cells labeled with [³H]choline together with 10-ASA shows that the majority of radioactivity is not incorporated into SM but in phosphatidylcholine, as described previously (5).

The conversion of photoSph to photoSM was confirmed by mass spectrometric analysis of lipid extracts obtained from labeled cells. As UV irradiation of the photolabile compound results in the release of nitrogen, the presence of photoactivatable SM can easily be followed by UV irradiation of lipid extracts and subsequent mass spectrometric analysis monitoring the loss of the original mass peak of photoactivatable SM. For mass spectrometric analysis, CHO cells were fed with nonradioactive D-erythro-photoSph. Lipid extracts were subjected to mild basic hydrolysis to break fatty acyl ester bonds and separated by TLC. TLC spots corresponding to SM were extracted from silica and analyzed by nano-ESI-MS/MS. To detect SM species, a precursor ion-scanning procedure for fragment ions of mass 184 Da was used, selectively monitoring lipid species containing a choline phosphate head group (184 Da). As lipid extracts were subjected to a mild basic treatment before mass spectrometric analysis, only SM and not phosphatidylcholine species were detected.

Figure 4A shows the molecular species composition of SM extracted from CHO cells that were kept for 3 h in delipidated αMEM. No difference was observed compared with cells kept in αMEM supplemented with fetal calf serum (data not shown). The administration of D-erythro-photoSph to the cell medium resulted in the appearance of additional peaks in the spectrum (Fig. 4B). UV irradiation of this lipid extract caused a loss of these peaks, identifying them as photoSM 16:0 and photoSM 24:1 (Fig. 4C). In agreement with the physiological situation, photoSM 16:0 is the major photoactivatable SM species.

Photoactivatable SM can be recovered from DRMs

Sphingolipids are essential components of DRMs. To investigate whether the photolabile diazirine group would interfere with the property of sphingolipids to enter DRMs, [³H]D-erythro-photoSph-labeled cells were treated with cold Triton X-100 and then subjected to an Optiprep density centrifugation. As illustrated in **Fig. 5A**, fractions were analyzed regarding the distribution of flotillin, a marker for the DRM fraction, and of p23, which is not associated with DRMs (10). Lipid extracts of the density gradient fractions were analyzed by TLC, and patterns of radioactive lipids were visualized by digital autoradiography. Photoactivatable SM, GM3, and Cer were recovered from the DRM fractions (data not shown). To compare the partitioning of photoactivatable lipids with their endogenous sphingolipid counterparts, DRMs were prepared from unlabeled cells. Thirty percent of SM was recovered
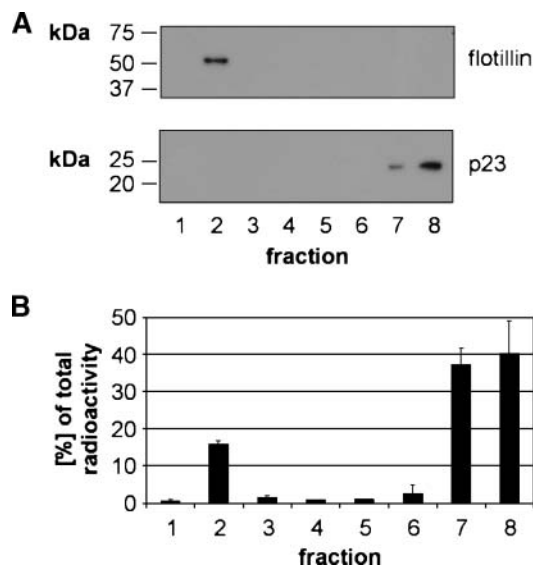
Fig. 5. Photolabile sphingolipids partition into detergent-resistant membranes (DRMs). A total of 1×10^7 CHO cells (two 10 cm dishes) were grown in the presence of 1 μM (200 μCi/10 ml and dish) [³H]D-erythro-photoSph for 6 h. After extraction with cold Triton X-100 at 4°C, samples were subjected to Optiprep density centrifugation as described. Gradients were fractionated from top to bottom into eight fractions. A: Gradient fractions were analyzed for DRM (flotillin) and detergent-soluble membranes (p23) by Western blotting. B: The radioactivity of each fraction was measured, and values are given as percentage of total radioactivity for all gradient fractions (n = 2). Error bars indicate ± SD.

from the DRM fraction (data not shown). In comparison, ~20% of total SM-derived radioactivity was recovered in the DRM fraction (Fig. 5B), indicating that the introduction of the photolabile diazirine group does not impede the partition into DRMs of photoactivatable lipids.

In vivo analysis of protein-sphingolipid interactions

To investigate the suitability of [³H]D-erythro-photoSph as a tool to probe the microenvironment of transmembrane proteins in vivo, cells were labeled with [³H]D-erythro-photoSph, [³H]choline/10-ASA, or MβCD-complexed [³H]photoChol, yielding photoactivatable sphingolipids, phosphatidylcholine, or cholesterol, respectively. For photoaffinity labeling studies, cells were irradiated with UV light to covalently link photoactivatable lipids to proteins in close proximity. Proteins were separated via SDS-PAGE and transferred to a PVDF membrane. Protein-lipid interactions were visualized by digital autoradiography. As shown in supplementary Fig. IV for [³H]D-erythro-photoSph, different patterns of proteins radioactively labeled with [³H]sphingolipids were obtained when various cell lines were compared.

To test whether [³H]photoSph can be used to study sphingolipid binding properties of proteins in vivo, we made use of CERT, mediating the transport of Cer from the endoplasmic reticulum to the Golgi (16). We transiently transfected COS7 cells with cDNA encoding FLAG-tagged CERT. After photoaffinity labeling, cells were UV-irradiated,

lysed, and subjected to immunoprecipitation using an anti-FLAG antibody. As illustrated in **Fig. 6**, the majority of radioactivity was recovered when cells were labeled by [³H]D-*erythro*-photoSph, confirming the specific sphingolipid-CERT interaction.

Caveolin-1 shows high affinities for cholesterol and sphingolipids

Because sphingolipids are enriched in rafts, we next wanted to test whether our probe could detect raft proteins as well. A bona fide raft marker is the 21 kDa protein caveolin-1, a key component in the formation of caveolae, which was shown to bind cholesterol (5, 17). To this end, we labeled CHO cells with [³H]D-*erythro*-photoSph and [³H]photoChol. Protein labeling patterns revealed some similarities (**Fig. 7A**, lanes 2, 10). A prominent radioactive

protein band with an apparent molecular mass of 21–24 kDa was present in both fractions. Because caveolin-1 binds cholesterol (5, 17), GM1 (18), and GM3 (19), we examined whether the 21–24 kDa band represents caveolin-1. Cell lysates were immunoprecipitated using an antibody directed against endogenous caveolin-1. Radioactivity was recovered from [³H]photoChol- and [³H]D-*erythro*-photoSph-labeled cells. However, only very low radioactivity was recovered from cells labeled with [³H]photoPC. Sphingolipid labeling of caveolin-1 was also observed when [³H]L-*threo*-photoSph was fed to cells, with the *threo* form being almost exclusively converted to SM and not to glycosphingolipids, as shown above. These results, together with the fact that CHO cells lack the capacity to synthesize glycosphingolipids higher that GM3 (20, 21) and the experimental conditions chosen to min-
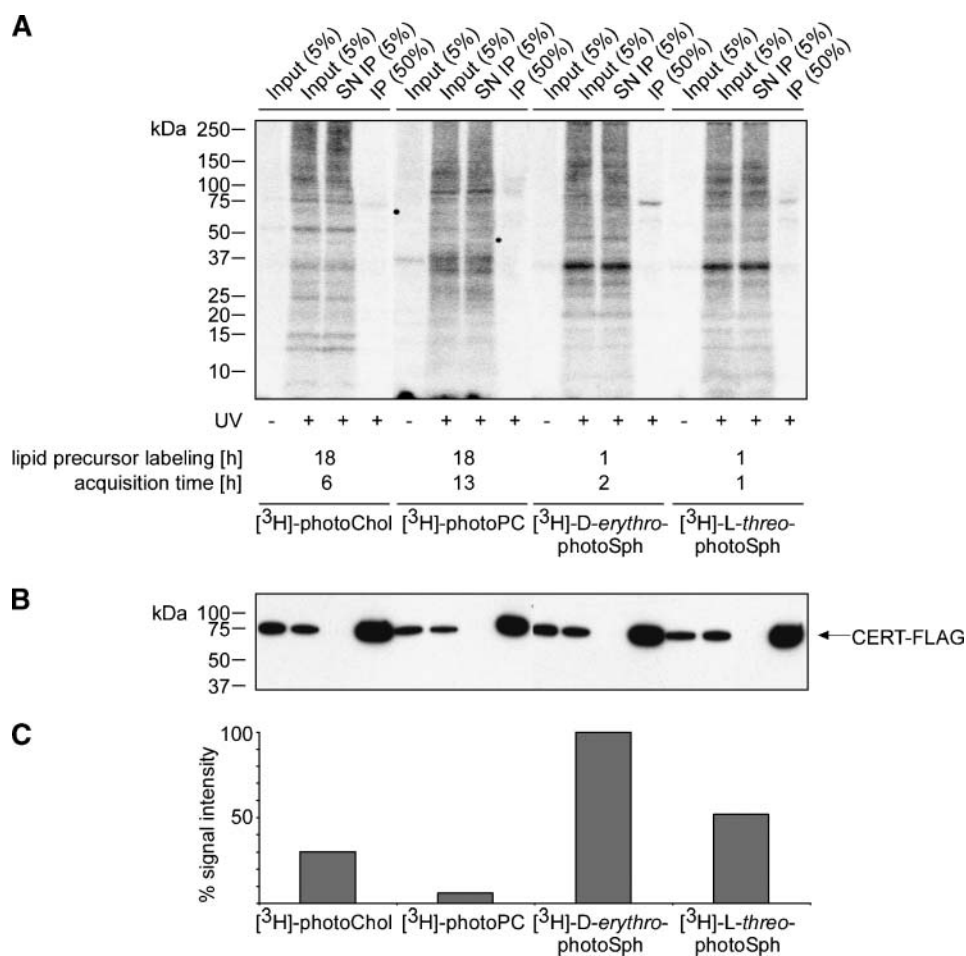

Fig. 6. Ceramide transporter (CERT) specifically interacts with sphingolipids but not with photo-cholesterol (photoChol) or photo-phosphatidylcholine (photoPC). COS7 cells were transiently transfected with a plasmid containing cDNA encoding FLAG-tagged CERT. Cells were grown in the presence of 200 μCi of methyl-β-cyclodextrin (MβCD)-complexed [³H]photoChol, [³H]choline/50 μM 10-ASA, [³H]D-*erythro*-photoSph, or [³H]L-*threo*-photoSph, with labeling times as indicated. At 23 h after transfection, cells were UV-irradiated, lysed, and subjected to immunoprecipitation using an anti-FLAG antibody. Samples of input (+/− UV irradiation), supernatant (SN), and pellet of immunoprecipitation (IP) were separated by SDS-PAGE and transferred to polyvinylidene difluoride (PVDF) membranes. A: Radioactively labeled proteins were visualized by digital autoradiography, with acquisition times as indicated. B: Western blot analysis using the anti-FLAG antibody. C: Quantitation of immunoprecipitated radioactivity. The values are given as percentages compared with the sample with highest radioactivity.
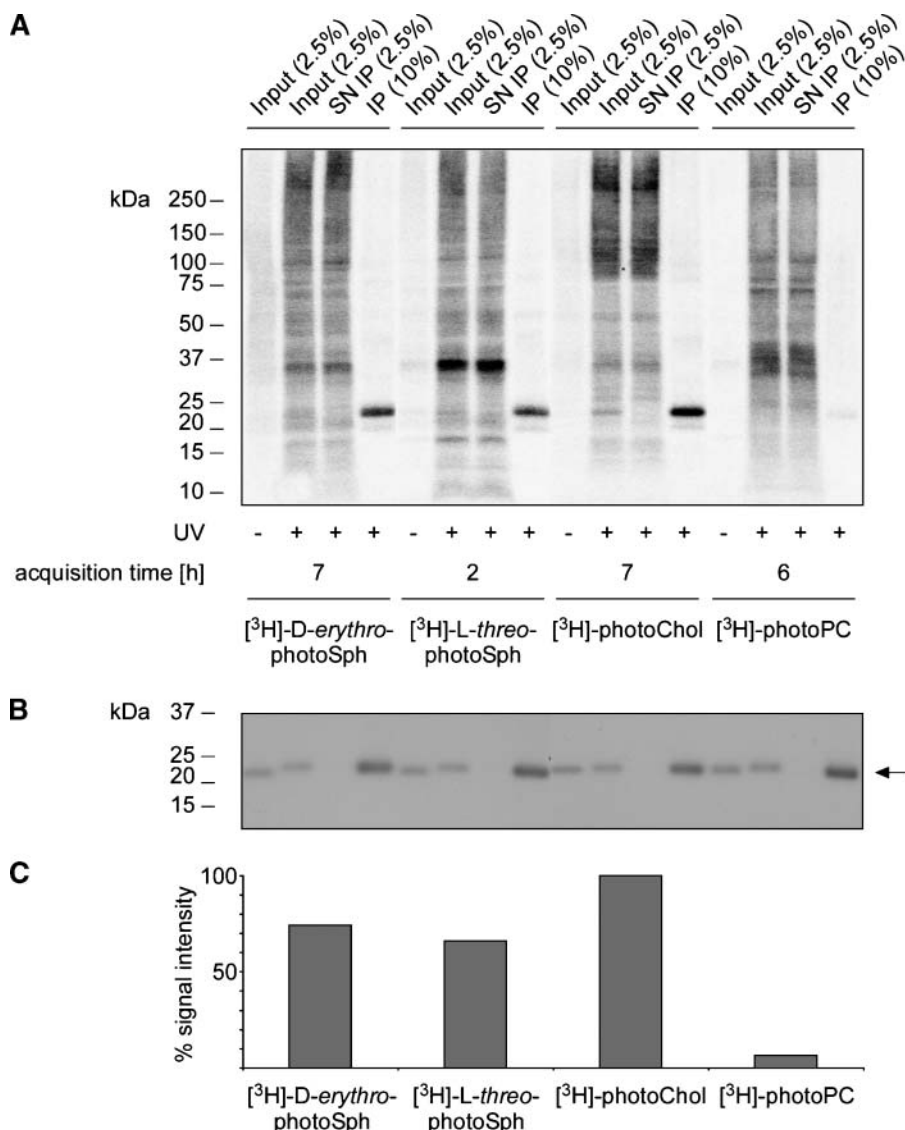
A

B

C

Fig. 7. Caveolin-1 interacts with cholesterol and sphingolipids. CHO cells were labeled for 20 h with 200 μCi of [^{3}H]D-*erythro*-photoSph, [^{3}H]L-*threo*-photoSph, MβCD-complexed [^{3}H]photoChol, or [^{3}H]choline/ 50 μM 10-ASA. After UV irradiation, cells were subjected to immunoprecipitation using an anti-caveolin antibody. Samples of input (+/− UV irradiation), supernatant (SN), and pellet of immunoprecipitation (IP) were separated by SDS-PAGE and transferred to PVDF membranes. A: Radioactively labeled proteins were visualized by digital autoradiography, with acquisition times as indicated. B: Western blot analysis using the anti-caveolin antibody. C: Quantitation of immunoprecipitated radioactivity. The values are given as percentages compared with the sample with highest radioactivity.

imize the labeling of Cer, indicate that caveolin-1 also interacts with SM.

Cytosolic PI-TPβ interacts with a sphingolipid

We next asked whether this sphingolipid probe could also detect lipid interactions with cytosolic lipid transfer proteins. To address this question, we made use of two cytosolic proteins that have been shown to bind SM in vitro. The phosphatidylinositol binding proteins PI-TPα and PI-TPβ were shown to bind phosphatidylinositol and phosphatidylcholine in vitro. In addition, PI-TPβ was shown to bind and transfer SM in vitro (22–24). To investigate whether PI-TPβ but not PI-TPα interacts with a

sphingolipid in vivo, we transiently transfected CHO cells with cDNA encoding either V5-tagged PI-TPβ or PI-TPα. At 20 h after transfection, cells were labeled with [^{3}H]D-*erythro*-photoSph. Cells were harvested and lysed, and cell lysates were subjected to immunoprecipitation. As shown in **Fig. 8A**, radioactivity was recovered in the purified fraction of PI-TPβ, demonstrating a direct protein-sphingolipid interaction in vivo. In addition, a weak interaction with PI-TPα was observed. Analysis of immunoprecipitated proteins from [^{3}H]photoChol- or [^{3}H]photoPC-labeled cells revealed that under both conditions, no radioactivity was recovered (Fig. 8C). The fact that no in vivo labeling of PI-TP with [^{3}H]photoPC was observed fits with recently
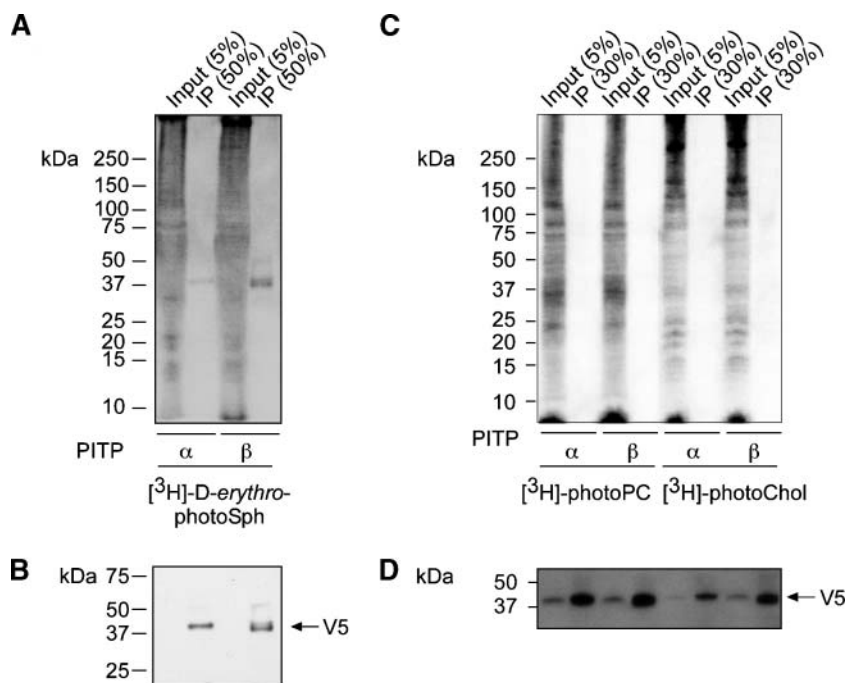
Fig. 8. In vivo interaction of phosphatidylinositol transfer protein (PI-TP) β with photolabile lipids. CHO cells were transiently transfected with constructs encoding V5-tagged PI-TPα and PI-TPβ. At 20 h after transfection, cells were labeled with 200 μCi of [³H]D-*erythro*-photoSph (A), [³H]photoChol (C), or [³H]choline/50 μM 10-ASA for 12 h (C). After UV irradiation, cell lysates were subjected to immunoprecipitation using an anti-V5 antibody. Samples of input and pellet of immunoprecipitation (IP) were separated by SDS-PAGE (10–20% Tris/Tricine gradient gels) and transferred to PVDF membranes. A, C: Radioactively labeled proteins were visualized by digital autoradiography, with an acquisition time of 5 h. B, D: Western blot analysis using the anti-V5 antibody.

reported in vivo fluorescence resonance energy transfer experiments (25) but is in conflict with the published in vitro data and remains to be further investigated.

Only the mature form of nicastrin interacts with a sphingolipid

Nicastrin together with presenilin, aph-1, and pen-2 constitute the core unit of the γ-secretase complex, the intermembrane protease that mediates the last step in the proteolytic processing of amyloid precursor protein and other transmembrane proteins (for a recent review, see Refs. 26, 27). Unlike presenilin, aph-1, and pen-2, nicastrin is inserted into the membrane by only a single transmembrane span. Depending on its glycosylation state, it exists in an immature and a mature form, with only the latter being associated with the active γ-secretase complex (28). In addition, it was recently shown that the assembly of the γ-secretase complex is accompanied by a major conformational change within nicastrin (29). Together, these data indicate a role of nicastrin in complex assembly.

To address the question of whether protein-lipid interactions might play a role in initiating the assembly process, we compared the direct lipid environments of both mature and immature nicastrin. To this end, human hippocampal SH-S5Y5 cells were incubated with the various photoactivatable lipid precursors. After UV irradiation, cells were lysed and subjected to a dissociative

immunoprecipitation to recover both complexed and uncomplexed nicastrin. Immunoprecipitates were subjected to SDS-PAGE and electroblotting. Recovery of radioactivity was analyzed by digital autoradiography. Irradiation of both [³H]photoChol- and [³H]D-*erythro*-photoSph-labeled cells led to cross-linking of only the mature form of nicastrin. In contrast, [³H]photoPC labeling resulted in cross-linking of both the mature and immature forms with comparable intensities (**Fig. 9**).

DISCUSSION

Here, we report the chemical synthesis of a novel radioactive and photoactivatable sphingosine derivative, [³H]D-*erythro*-photoSph. We show specific interaction with the established Cer binding protein CERT and elucidate novel specific interactions with caveolin-1, PI-TPβ, and the mature form of nicastrin.

A variety of photolabile sphingolipids have been used successfully to detect protein-lipid interactions outside the hydrophobic lipid bilayer (e.g., to study the interaction of soluble proteins with carbohydrate groups of glycosphingolipids) (2). Detection of sphingolipid interactions in the lipid bilayer was hampered because the modified sphingolipid contained a fatty acid with a bulky photolabile group that could affect the typical behavior of the sphin-
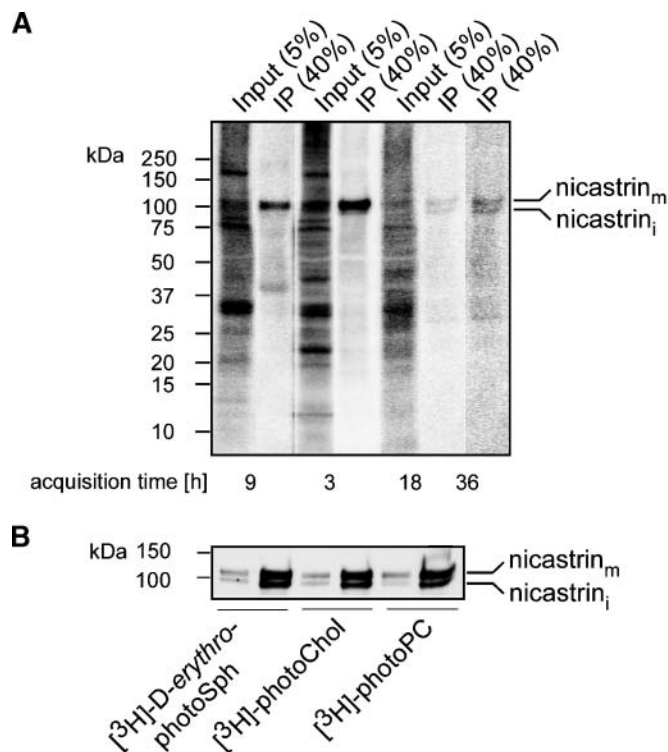
Fig. 9. Lipid labeling of nicastrin. Fifteen centimeter dishes of SH-SY5Y cells were labeled for 6 h ($[^3H]$D-erythro-photoSph) or 18 h ($[^3H]$photoChol and $[^3H]$choline chloride/10-ASA) with 400 μCi of $[^3H]$D-erythro-photoSph, $[^3H]$photoChol, or $[^3H]$choline chloride/10-ASA. Cells were transferred to ice, washed with PBS, and subjected to 10 min of UV irradiation. After UV irradiation, cells were scraped off and lysed as described. Lysates were subjected to a dissociative immunoprecipitation using an anti-nicastrin antibody. Nicastrin$_m$, mature form of nicastrin; nicastrin$_i$, immature form of nicastrin. Five percent of input and 40% of the immunoprecipitated samples (IP) were separated by SDS-PAGE using a 10–20% Tris/Tricine gradient gel. A: After transfer of proteins to PVDF membranes, radioactively labeled proteins were visualized by digital autoradiography as described, with acquisition times as indicated. B: Immunodetection was performed using an antibody directed against nicastrin.

golipid. We describe the introduction of a photolabile diazirine group within the sphingoid backbone that only slightly alters the overall structure of the sphingolipid analog. In addition, it has the advantage of modifying all of molecular species of each sphingolipid class. Owing to the positions of the photoactive diazirine group and the radioactive label, $[^3H]$photoSph allows the detection of protein-sphingolipid interactions exclusively, as no radioactive and photolabile metabolic intermediates other than sphingolipids are generated (see supplementary Fig. V).

Like its natural counterpart $[^3H]$D-erythro-sphingosine, $[^3H]$D-erythro-photoSph is rapidly metabolized to photoactive sphingolipids. Because of a potential apoptotic effect of increased Cer levels, exogenously added sphingosine was usually administered in a concentration not exceeding 0.1–5 μM, with no observable effects on cell growth and viability.

Photoactivatable sphingolipids are incorporated in cellular membranes and partition into DRMs, indicating that they mimic the biophysical properties of endogenous sphingolipids.

To investigate whether $[^3H]$D-erythro-photoSph can be used to photoaffinity-label proteins with radioactive sphingolipids, as a proof of principle we analyzed specific lipid interactions of CERT. Using the $[^3H]$D-erythro-photoSph sphingolipid precursor, we show an in vivo interaction of CERT with a sphingolipid. To analyze the specificity of CERT to interact with a sphingolipid, cells were additionally labeled with $[^3H]$photoChol or $[^3H]$choline/10-ASA. $[^3H]$choline/10-ASA labeling mainly generates photoactive phosphatidylcholine species. Labeling conditions were chosen that result in the labeling of Cer. Using these lipid precursors, we show that CERT exhibits a high affinity for sphingolipids but not for phosphatidylcholine or cholesterol. CERT labeling was also observed when cells were labeled with $[^3H]$L-threo-photoSph. However, the radioactive labeling of CERT with $[^3H]$L-threo-photoSph was lower than that for $[^3H]$D-erythro-photoSph, consistent with a lower transfer activity of CERT with C_{16}-L-threo-Cer (30).

A comparison of radioactive protein patterns from labeling experiments with $[^3H]$D-erythro-photoSph and $[^3H]$photoChol revealed similarities. In both cases, a prominent band with an apparent molecular mass of 20–22 kDa can be found. Because the 22 kDa protein caveolin-1 is known for its strong affinity to bind cholesterol, we analyzed this interaction by in vivo $[^3H]$photoChol labeling. As expected, caveolin-1 interacts with cholesterol. Likewise, we identified the prominent sphingolipid-labeled cellular protein to be caveolin-1, demonstrating that caveolin-1 not only binds cholesterol but also possesses a high affinity for sphingolipids. As the labeling of caveolin-1 with $[^3H]$L-threo-photoSph was also observed in CHO cells lacking GM1, and because, with the given labeling conditions, the main radioactive photolabile lipid class containing this photolabile sphingolipid precursor is $[^3H]$photoSM, we conclude that caveolin-1 interacts with SM. It remains to be investigated whether the interaction of SM is of a preferential nature (and thus would take place even in a membrane with low amounts of SM, such as the endoplasmic reticulum) and whether caveolin binds both SM and cholesterol at the same time.

To test whether the sphingolipid probe can also be used to probe the interactions of cytosolic proteins with lipids, we chose the lipid transfer protein PI-TP. In vitro experiments show that PI-TPβ is able to transfer SM between membranes. Here, we show that PI-TPβ binds to sphingolipids in vivo, indicating that some SM resides in the cytosolic leaflet of cellular membranes.

We next used the photoactivatable lipids to probe the molecular environment of mature and immature nicastrin. Nicastrin is part of the active γ-secretase complex, which is involved in the intermembrane proteolysis of type I transmembrane proteins, such as amyloid precursor protein and Notch (for recent reviews, see Refs. 26, 27). Expression of the four transmembrane core proteins is tightly controlled; however, little is known about the molecular mechanisms of assembly into the intact, active

γ-secretase complex. Recent data suggest that nicastrin plays a central role not only in assembling the complex but also in substrate recognition (31). Nicastrin is a glycosylated protein integrated into the lipid bilayer by a single transmembrane span. Depending on the glycosylation state, a mature and an immature form of nicastrin exist. Interestingly, only the fully assembled γ-secretase complex passes the secondary quality control of the early secretory pathway, resulting in presenilin cleavage and nicastrin maturation. Thus, the amount of mature nicastrin might be regarded as an indicator for the active γ-secretase complex. In the present study, we show that labeling of SH-SY5Y cells with both [³H]photoChol and [³H]D-erythro-photoSph and UV irradiation result in a cross-linking exclusively of the mature form of nicastrin. In contrast, [³H]photoPC labeling gives rise to a cross-link with both the mature and immature forms of nicastrin. These data indicate that mature and immature nicastrin reside in membrane environments distinct from each other. Furthermore, these results suggest a novel role of specific nicastrin-lipid interactions in complex assembly and/or the modulation of γ-secretase activity.

Lipids are increasingly being recognized not only as constituents of cell membranes but also as key factors in intracellular trafficking, signaling, and diseases such as cancer, HIV infection, and Alzheimer's. Photoaffinity labeling using photoChol or [³H]choline/10-ASA has been a very efficient tool for studying protein-cholesterol and protein-phosphatidylcholine interactions (5, 32–35). Now, [³H]photoSph provides researchers with a novel tool to study protein-lipid interactions in vivo. With these tools, an even higher level of molecular insight will be possible once methods are developed for highly sensitive mass spectrometric analysis of protein-lipid adducts. Eventually, this will reveal the individual molecular lipid species bound. Meanwhile, with the information obtained from labeling studies performed using the photolabile lipid precursors described above, specific lipid probes (i.e., with defined fatty acid compositions) can help to identify the molecular lipid species bound.▯

REFERENCES

1. Snook, C. F., J. A. Jones, and Y. A. Hannun. 2006. Sphingolipid-binding proteins. *Biochim. Biophys. Acta.* **1761:** 927–946.
2. Knoll, F., T. Kolter, and K. Sandhoff. 2000. Sphingolipid photo-affinity labels. *Methods Enzymol.* **311:** 568–600.
3. Elsen, L., R. Betz, G. Schwarzmann, K. Sandhoff, and G. van Echten-Deckert. 2002. Identification of ceramide binding proteins in neuronal cells: a critical point of view. *Neurochem. Res.* **27:** 717–727.
4. Zegers, M. M., J. W. Kok, and D. Hoekstra. 1997. Use of photo-activatable sphingolipid analogues to monitor lipid transport in mammalian cells. *Biochem. J.* **328:** 489–498.
5. Thiele, C., M. J. Hannah, F. Fahrenholz, and W. B. Huttner. 2000. Cholesterol binds to synaptophysin and is required for biogenesis of synaptic vesicles. *Nat. Cell Biol.* **2:** 42–49.
6. Hait, N. C., C. A. Oskeritzian, S. W. Paugh, S. Milstien, and S. Spiegel. 2006. Sphingosine kinases, sphingosine 1-phosphate, apoptosis and diseases. *Biochim. Biophys. Acta.* **1758:** 2016–2026.
7. Pettus, B. J., C. E. Chalfant, and Y. A. Hannun. 2002. Ceramide in apoptosis: an overview and current perspectives. *Biochim. Biophys. Acta.* **1585:** 114–125.
8. Taha, T. A., T. D. Mullen, and L. M. Obeid. 2006. A house divided: ceramide, sphingosine, and sphingosine-1-phosphate in programmed cell death. *Biochim. Biophys. Acta.* **1758:** 2027–2036.
9. Jenne, N., K. Frey, B. Brügger, and F. T. Wieland. 2002. Oligomeric state and stoichiometry of p24 proteins in the early secretory pathway. *J. Biol. Chem.* **277:** 46504–46511.
10. Gkantiragas, I., B. Brügger, E. Stuven, D. Kaloyanova, X. Y. Li, K. Lohr, F. Lottspeich, F. T. Wieland, and J. B. Helms. 2001. Sphingomyelin-enriched microdomains at the Golgi complex. *Mol. Biol. Cell.* **12:** 1819–1833.
11. Brügger, B., B. Glass, P. Haberkant, I. Leibrecht, F. T. Wieland, and H. G. Krausslich. 2006. The HIV lipidome: a raft with an unusual composition. *Proc. Natl. Acad. Sci. USA.* **103:** 2641–2646.
12. Ramstedt, B., and J. P. Slotte. 2000. Separation and purification of sphingomyelin diastereomers by high-performance liquid chromatography. *Anal. Biochem.* **282:** 245–249.
13. Pagano, R. E., and O. C. Martin. 1988. A series of fluorescent N-acylsphingosines: synthesis, physical properties, and studies in cultured cells. *Biochemistry.* **27:** 4439–4445.
14. van der Bijl, P., M. Lopes-Cardozo, and G. van Meer. 1996. Sorting of newly synthesized galactosphingolipids to the two surface domains of epithelial cells. *J. Cell Biol.* **132:** 813–821.
15. Venkataraman, K., and A. H. Futerman. 2001. Comparison of the metabolism of L-erythro- and L-threo-sphinganines and ceramides in cultured cells and in subcellular fractions. *Biochim. Biophys. Acta.* **1530:** 219–226.
16. Hanada, K., K. Kumagai, S. Yasuda, Y. Miura, M. Kawano, M. Fukasawa, and M. Nishijima. 2003. Molecular machinery for non-vesicular trafficking of ceramide. *Nature.* **426:** 803–809.
17. Murata, M., J. Peranen, R. Schreiner, F. Wieland, T. V. Kurzchalia, and K. Simons. 1995. VIP21/caveolin is a cholesterol-binding protein. *Proc. Natl. Acad. Sci. USA.* **92:** 10339–10343.
18. Fra, A. M., M. Masserini, P. Palestini, S. Sonnino, and K. Simons. 1995. A photo-reactive derivative of ganglioside GM1 specifically cross-links VIP21-caveolin on the cell surface. *FEBS Lett.* **375:** 11–14.
19. Chigorno, V., P. Palestini, M. Sciannamblo, V. Dolo, A. Pavan, G. Tettamanti, and S. Sonnino. 2000. Evidence that ganglioside enriched domains are distinct from caveolae in MDCK II and human fibroblast cells in culture. *Eur. J. Biochem.* **267:** 4187–4197.
20. Briles, E. B., E. Li, and S. Kornfeld. 1977. Isolation of wheat germ agglutinin-resistant clones of Chinese hamster ovary cells deficient in membrane sialic acid and galactose. *J. Biol. Chem.* **252:** 1107–1116.
21. Yogeeswaran, G., R. K. Murray, and J. A. Wright. 1974. Glyco-sphingolipids of wild-type and mutant lectin-resistant Chinese hamster ovarian cells. *Biochem. Biophys. Res. Commun.* **56:** 1010–1016.
22. de Vries, K. J., A. A. Heinrichs, E. Cunningham, F. Brunink, J. Westerman, P. J. Somerharju, S. Cockcroft, K. W. Wirtz, and G. T. Snoek. 1995. An isoform of the phosphatidylinositol-transfer protein transfers sphingomyelin and is associated with the Golgi system. *Biochem. J.* **310:** 643–649.
23. Li, H., J. M. Tremblay, L. R. Yarbrough, and G. M. Helmkamp, Jr. 2002. Both isoforms of mammalian phosphatidylinositol transfer protein are capable of binding and transporting sphingomyelin. *Biochim. Biophys. Acta.* **1580:** 67–76.
24. Segui, B., V. Allen-Baume, and S. Cockcroft. 2002. Phosphatidyl-inositol transfer protein beta displays minimal sphingomyelin transfer activity and is not required for biosynthesis and trafficking of sphingomyelin. *Biochem. J.* **366:** 23–34.
25. Larijani, B., V. Allen-Baume, C. P. Morgan, M. Li, and S. Cockcroft. 2003. EGF regulation of PITP dynamics is blocked by inhibitors of phospholipase C and of the Ras-MAP kinase pathway. *Curr. Biol.* **13:** 78–84.
26. Kaether, C., C. Haass, and H. Steiner. 2006. Assembly, trafficking and function of gamma-secretase. *Neurodegener. Dis.* **3:** 275–283.
27. Wolfe, M. S. 2006. The gamma-secretase complex: membrane-embedded proteolytic ensemble. *Biochemistry.* **45:** 7931–7939.
28. Yang, D. S., A. Tandon, F. Chen, G. Yu, H. Yu, S. Arawaka, H. Hasegawa, M. Duthie, S. D. Schmidt, T. V. Ramabhadran, et al.

2002. Mature glycosylation and trafficking of nicastrin modulate its binding to presenilins. *J. Biol. Chem.* **277:** 28135–28142.

29. Shirotani, K., D. Edbauer, A. Capell, J. Schmitz, H. Steiner, and C. Haass. 2003. Gamma-secretase activity is associated with a conformational change of nicastrin. *J. Biol. Chem.* **278:** 16474–16477.

30. Kumagai, K., S. Yasuda, K. Okemoto, M. Nishijima, S. Kobayashi, and K. Hanada. 2005. CERT mediates intermembrane transfer of various molecular species of ceramides. *J. Biol. Chem.* **280:** 6488–6495.

31. Shah, S., S. F. Lee, K. Tabuchi, Y. H. Hao, C. Yu, Q. LaPlant, H. Ball, C. E. Dann, 3rd, T. Sudhof, and G. Yu. 2005. Nicastrin functions as a gamma-secretase-substrate receptor. *Cell.* **122:** 435–447.

32. Eroglu, C., B. Brügger, F. Wieland, and I. Sinning. 2003. Glutamate-binding affinity of Drosophila metabotropic glutamate receptor is modulated by association with lipid rafts. *Proc. Natl. Acad. Sci. USA.* **100:** 10219–10224.

33. Matyash, V., C. Geier, A. Henske, S. Mukherjee, D. Hirsh, C. Thiele, B. Grant, F. R. Maxfield, and T. V. Kurzchalia. 2001. Distribution and transport of cholesterol in *Caenorhabditis elegans. Mol. Biol. Cell.* **12:** 1725–1736.

34. Olayioye, M. A., S. Vehring, P. Muller, A. Herrmann, J. Schiller, C. Thiele, G. J. Lindeman, J. E. Visvader, and T. Pomorski. 2005. StarD10, a START domain protein overexpressed in breast cancer, functions as a phospholipid transfer protein. *J. Biol. Chem.* **280:** 27436–27442.

35. Simons, M., E. M. Kramer, C. Thiele, W. Stoffel, and J. Trotter. 2000. Assembly of myelin by association of proteolipid protein with cholesterol- and galactosylceramide-rich membrane domains. *J. Cell Biol.* **151:** 143–154.